

Supporting Information

Murin et al. 10.1073/pnas.1414164111

SI Materials and Methods

Biolayer Interferometry Competition Binding Assay. All binding experiments were performed using the ForteBio Octet platform. All data were collected at 25 °C. Streptavidin-coated biosensor tips (ForteBio) were first equilibrated for 10 min in 1× PBS buffer (137 mM NaCl, 2.7 mM KCl, 10 mM Na₂HPO₄, and 2 mM KH₂HPO₄, pH 7.4) containing 0.1% (wt/vol) BSA and 0.02% (vol/vol) Tween 20, which will now be referred to as Kinetics Buffer. A baseline was then measured for 60 s following by immobilization of EBOV GPΔTM containing a C-terminal double streptavidin tag (Qiagen; see below) (25 μg/mL) for 2 min, a short wash in Kinetics Buffer for 60 s, and then a second baseline for 3 min. Antibody 1 (diluted to 1 μM in Kinetics Buffer) was next allowed to bind to immobilized GPΔTM for 15 min to saturation. Next, antibody 2 was allowed to also bind for 15 min. The percent binding of the competing mAb in the presence of the first mAb was determined by comparing the maximal signal of competing mAb applied after the first mAb complex to the maximal signal of competing mAb alone. mAbs were considered competing for the same site if maximum binding of antibody 2 was reduced to <10% of its noncompeted binding (black boxes). mAbs were considered noncompetitive if maximum binding of antibody 2 was >30% of its binding to GP alone (white boxes). Gray boxes indicate an intermediate phenotype (between 10% and 30% of uncompetited binding; Fig. 1). The decreased responses observed during injection of antibody 2 in many of the titrations is likely due to either lack of saturation of the biosensor by antibody 1 and/or dissociation of antibody 1. Due to these phenomena, along with potential avidity effects due to injection of IgG (two binding sites per molecule), we only interpreted these data in a qualitative manner. Importantly, despite these concerns, the data are highly consistent with our structural observations.

Expression and Purification of EBOV GPs. Recombinant EBOV GP ectodomains containing the mucin-like domain (EBOV GPΔTM) or lacking residues 312–463 of the mucin-like domain (EBOV GPΔmuc) (1, 2) were produced by transfection of *Drosophila* Schneider 2 (S2) cells with modified pMTpuro vectors, followed by stable selection of transfected cells with 6 μg/mL puromycin. Secreted GP ectodomain expression was induced with 0.5 mM CuSO₄ for 4 d. Proteins were engineered with a modified double strep tag at the C terminus (enterokinase cleavage site followed by a strep tag/linker/strep tag) to facilitate purification using Strep-Tactin resin (Qiagen). Proteins were purified further by Superdex 200 (S200) SEC in 10 mM Tris and 150 mM NaCl, pH 7.5 (1× TBS).

Plant-Derived mAb and Fab Production and Purification. Plant-derived mAbs were kindly provided by Mapp Biopharmaceuticals and Kentucky Bioprocessing. IgGs were engineered, expressed, and purified as described previously (3–6). To generate Fab fragments suitable for EM complexes, optimized papain digestion was used. IgGs were diluted to 1 mg/mL in 100 mM Tris and 2 mM EDTA, pH 8.0 (1× TE) with 10 mM L-cysteine and 4% (wt/vol) activated

papain and allowed to incubate at 37 °C for 6 h. Digestion was stopped with addition of 50 mM iodacetamide. Digests were then loaded onto a 5-mL Hi-Trap Protein A column (GE) equilibrated with 1× PBS, and the flow-through was collected. Fabs were further purified by S200 SEC in 1× TBS, pH 7.4.

EM and Sample Preparation. Fabs were added in molar excess to GPΔTM and allowed to incubate overnight at 4 °C. Complexes were then purified by S200 SEC in 1× TBS, pH 7.4. For ternary complexes (those with two different Fabs bound), the second Fab was added in molar excess after purification of the first complex and applied directly onto grids. To prepare negative-stain grids, a 4-μL aliquot of each complex, which had been diluted to a concentration of ~0.03 μg/mL with TBS buffer, was placed for 15 s onto carbon-coated 400-Cu mesh grids that had been plasma cleaned for 20 s (Gatan), blotted off on the edge of the grid, and then immediately stained for 30 s with 4 μL of 2% (wt/vol) uranyl formate. The stain was blotted off on the edge of the grid, and the grid was allowed to dry. Data were automatically collected with Legicon (7–9) using a FEI Tecnai F20 electron microscope operating at 120 keV with an electron dose of 30 e⁻/Å² and a magnification of 52,000× that resulted in a pixel size of 2.65 or 2.05 Å at the specimen plane when collected with Tietz CMOS 4k × 4k CCD camera. Particle orientations appeared to be generally isotropic and images were acquired at a constant defocus value of -1.0 μm at 0° stage tilt.

Image Processing. Particles were picked automatically using DoG Picker (10) and placed into a particle stack using the Appion software (11). Reference-free 2D class averages were generated with the Xmipp clustering 2D alignment software (12) and sorted into an initial 300 classes. Non-GP particles were removed and the stack was further subclassified into classes with ~100 particles per class to generate the final particle stack used for the reconstruction. Various numbers of class averages were chosen to create initial models using EMAN2 common lines software (13). A model that best matched its projected classes was then used for refinement against the raw particle stack, imposing C3 symmetry, and the reconstruction was generated with 10 rounds of refinement and increasingly smaller angular sampling rates with EMAN2 (13). All model fitting and manipulation was completed using UCSF Chimera (14).

Site-Directed Mutagenesis. Site-directed mutagenesis in GP was performed using the Quick Change site-directed mutagenesis kit (Agilent), with all mutations confirmed by sequencing (Eton).

ELISA with Q508R Mutant. GPΔmuc containing the desired mutation and a C-terminal HA-antibody tag was created by transient transfection of 293F cells as described previously (1). Supernatants containing GPΔmuc diluted 1:1 in 1× PBS + 0.05% BSA were allowed to coat plates for 1 h. Antibodies were then allowed to bind at a concentration of 2 μg/mL for 1 h. Binding was detected with an anti-human IgG HRP-coupled antibody using a plate reader.

- Lee JE, et al. (2008) Structure of the Ebola virus glycoprotein bound to an antibody from a human survivor. *Nature* 454(7201):177–182.
- Lee JE, et al. (2009) Techniques and tactics used in determining the structure of the trimeric ebolavirus glycoprotein. *Acta Crystallogr D Biol Crystallogr* 65(Pt 11):1162–1180.
- Zeitlin L, et al. (2011) Enhanced potency of a fucose-free monoclonal antibody being developed as an Ebola virus immunoprotectant. *Proc Natl Acad Sci USA* 108(51):20690–20694.
- Olinger GG, Jr, et al. (2012) Delayed treatment of Ebola virus infection with plant-derived monoclonal antibodies provides protection in rhesus macaques. *Proc Natl Acad Sci USA* 109(44):18030–18035.
- Giritch A, et al. (2006) Rapid high-yield expression of full-size IgG antibodies in plants coinfecting with noncompeting viral vectors. *Proc Natl Acad Sci USA* 103(40):14701–14706.
- Strasser R, et al. (2008) Generation of glyco-engineered *Nicotiana benthamiana* for the production of monoclonal antibodies with a homogeneous human-like N-glycan structure. *Plant Biotechnol J* 6(4):392–402.
- Carragher B, et al. (2000) Legicon: An automated system for acquisition of images from vitreous ice specimens. *J Struct Biol* 132(1):33–45.
- Potter CS, et al. (1999) Legicon: A system for fully automated acquisition of 1000 electron micrographs a day. *Ultramicroscopy* 77(3-4):153–161.

- Suloway C, et al. (2005) Automated molecular microscopy: The new Legikon system. *J Struct Biol* 151(1):41–60.
- Voss NR, Yoshioka CK, Radermacher M, Potter CS, Carragher B (2009) DoG Picker and TiltPicker: software tools to facilitate particle selection in single particle electron microscopy. *J Struct Biol* 166(2):205–213.
- Lander GC, et al. (2009) Appion: An integrated, database-driven pipeline to facilitate EM image processing. *J Struct Biol* 166(1):95–102.
- van Heel M, Harauz G, Orlova EV, Schmidt R, Schatz M (1996) A new generation of the IMAGIC image processing system. *J Struct Biol* 116(1):17–24.
- Tang G, et al. (2007) EMAN2: An extensible image processing suite for electron microscopy. *J Struct Biol* 157(1):38–46.
- Pettersen EF, et al. (2004) UCSF Chimera—a visualization system for exploratory research and analysis. *J Comput Chem* 25(13):1605–1612.

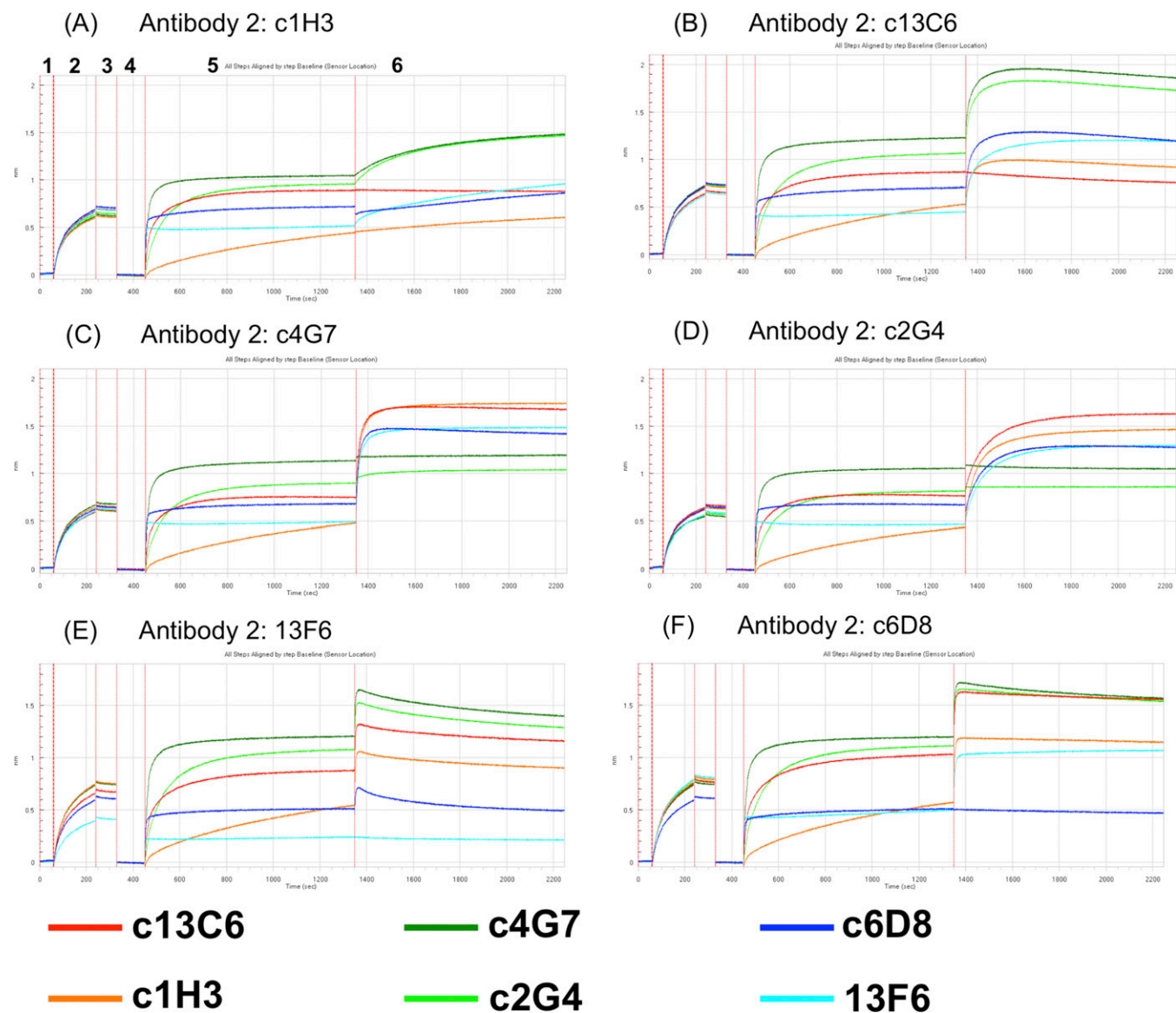


Fig. S1. Binding curves for reported competition assay results. Colored curves are the experimental trace obtained from bio-layer interferometry. In A, numbers indicate the following steps: (1) biosensor baseline, (2) GP loading, (3) GP wash, (4) baseline 2 (corrected), (5) antibody 1 loading, (6) antibody 2 loading. mAbs are indicated by key at the bottom of the figure. Saturation points (in response units) at the end of steps 5 and 6 were used to calculate competition values. B–F are the same as in A for each indicated antibody.

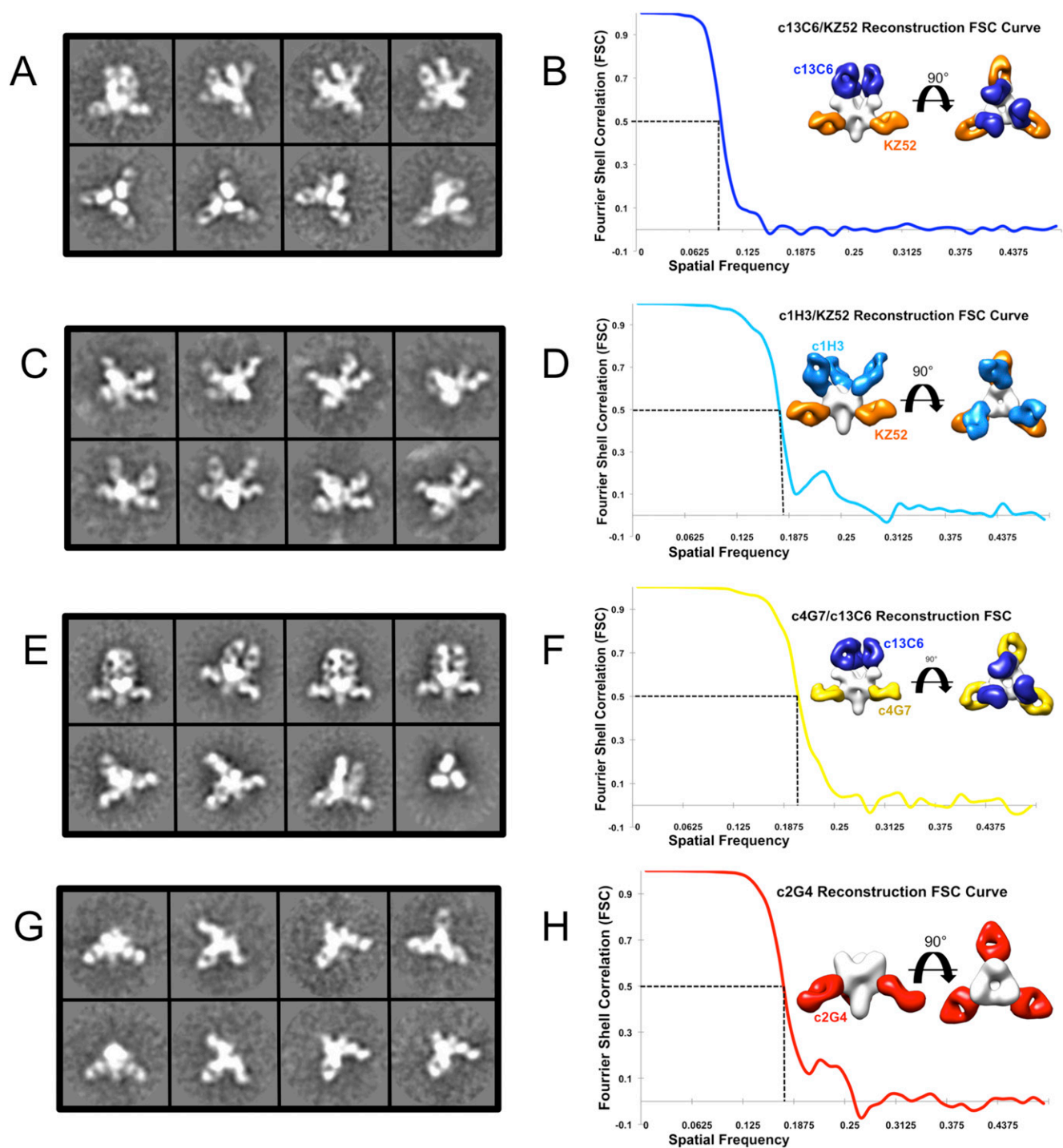


Fig. S2. Negative-stain EM data. (A) Representative negative-stain 2D class averages of the c13C6 Fab:KZ52 Fab:GPΔTM sample. (B) Fourier shell correlation (FSC) curve used to determine the resolution of the final reconstruction (Table S1). The full reconstruction is shown with side (Left) and top (Right) views. c13C6 is colored in blue and KZ52 Fab is in orange. (C and D) As in A and B but for the c1H3Fab:KZ52 Fab:GPΔTM reconstruction. c1H3 Fab is in light blue and KZ52 Fab is in orange. (E and F) As in A and B but for the c13C6 Fab:c4G7 Fab:GPΔTM reconstruction. c13C6 Fab is in blue and c4G7 Fab is in yellow. (G and H) As in A and B but for the c2G4:GPΔTM reconstruction. c2G4 Fab is in red. GPΔTM for each reconstruction is in white.

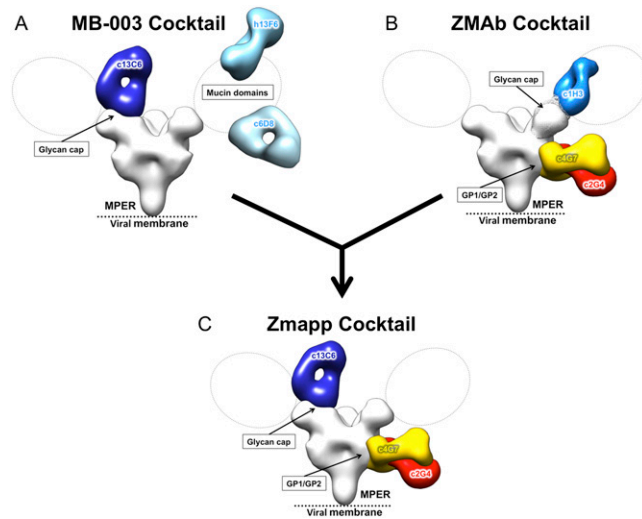


Fig. S3. Comparison of MB-003, ZMAb, and ZMapp antibody mixtures. (A) A negative-stain reconstruction of MB-003, including c13C6 (dark blue) in complex with EBOV GP Δ TM (from the reconstruction in complex with c4G7, which was removed from the model) and a rendering of Fabs h13F6 (cyan) and c6D8 (light blue), which bind the flexible mucin-like domain, demonstrating how all three mAbs bind regions which are removed before viral entry. (B) Negative-stain reconstructions of ZMAb, including c1H3 (medium blue, from the reconstruction in complex with KZ52, which was removed from the model), c4G7 (yellow, from the reconstruction in complex with c13C6, which was removed from the model), and c2G4 (red) in complex with EBOV GP Δ TM were combined to create a hybrid model of the ZMAb mixture, demonstrating how all three mAbs bind the core GP. (C) Reconstructions of the MB-003 and ZMAb mixtures allowed the creation of a hybrid model of the ZMapp mixture, which includes c13C6 (dark blue), c4G7 (yellow) and c2G4 (red), demonstrating the similarity of ZMapp to ZMAb with the exception of the glycan cap antibody angle of approach. MPER, membrane proximal external region.

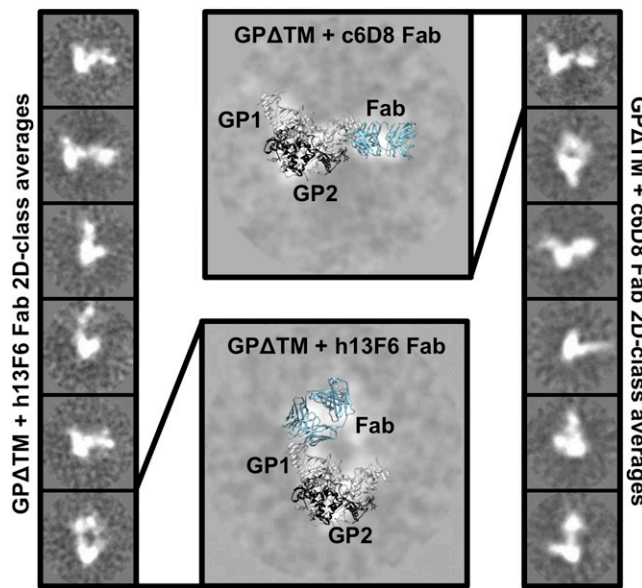


Fig. S4. Negative-stain 2D class averages of fixed 13F6 Fab:GP Δ TM and c6D8:GP Δ TM complexes. Complexes of the two mucin-domain binding mAbs with GP Δ TM were purified, fixed with 0.125% glutaraldehyde, and visualized by negative-stain EM. Representative class averages are shown for each complex with examples of each enhanced and then fit with a structure of GP Δ muc and a representative Fab (PDB ID code 3CSY) to orient the location of each portion of the respective complex.

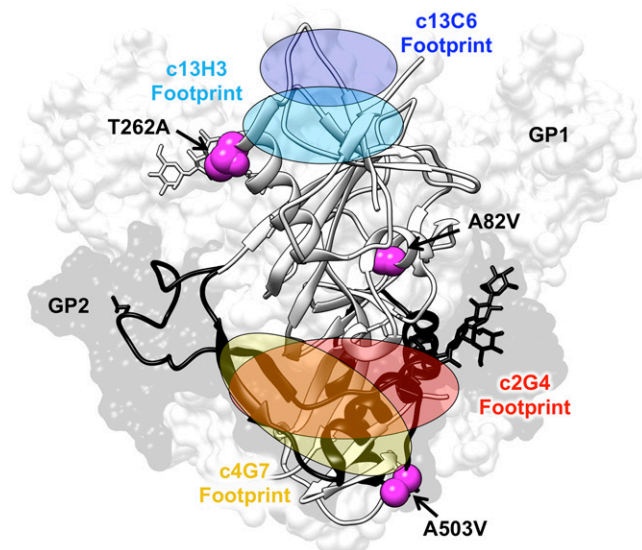


Fig. S5. Map of GP mutations from West African 2014 outbreak Zaire strain. Mutations of core GP (outside the mucin-like domains) that appeared in at least two isolates from the West Africa 2014 Zaire strain, and that differ from the 1995 Kikwit strain of Ebola virus, are mapped onto the structure of GP Δ muc in magenta (PDB ID code 3CSY) (1). The antibody footprints of c13C6 and c1H3 mAbs, which bind to the glycan cap (in cool colors) and c4G7 and c2G4 mAbs, which bind to the GP1-GP2 interface (in warm colors), are shown overlaid onto the map, indicating that mutations from the West African 2014 outbreak do not lie within significant portions of the ZMab or MB-003 core antibodies, within the limits of our reconstructions (\sim 20-Å resolution).

1. Gire SK, et al. (2014) Genomic surveillance elucidates Ebola virus origin and transmission during the 2014 outbreak. *Science* 345(6202):1369–1372.

Table S1. EM reconstruction statistics

Model	Number of particles in refinement	Final pixel size (1/Å)	Resolution (Å)	EMDB ID
EBOV GP Δ TM:c13C6 Fab:KZ52 Fab	8,367	2.05	22	6153
EBOV GP Δ TM:c1H3 Fab:KZ52 Fab	2,411	2.05	24	6150
EBOV GP Δ TM:c4G7 Fab:c13C6 Fab	10,210	2.05	21	6152
EBOV GP Δ TM:c2G4 Fab	5,772	2.05	24	6151

The table shows the number of particles and pixel size used for each refinement. Resolutions indicated for each map were determined at an FSC cutoff of 0.5 (Fig. S1).

Table S2. ELISA of GP Δ TM:Q508R mutant

Column1	WT GP Δ Muc	GP Δ Muc:Q508R	BSA
KZ52 IgG	1.9	0.16	0.24
c2G4 IgG	1.5	0.17	0.18
antiHA	1.9	1.9	0.16

To determine if the escape mutation Q508R (identified in a primate treated with ZMab which had succumbed to infection), which falls within the epitopes of c2G4 and c4G7, affects the binding of KZ52, we generated GP Δ muc with this point mutation by site-directed mutagenesis and assayed binding by ELISA. As predicted by our structural data, the Q508R mutation also restricts the binding of KZ52. GP Δ muc, mucin-deleted GP.

Table S3. Comparison of protective ebolavirus mAbs

Antibody	Virus	Ref.	Year	Source	Original isotype	Epitope region
KZ52	EBOV	1	1999	Human survivor	Human IgG1	GP1/GP2
4G7	EBOV	2	2011	VSV/EBOV GP mouse vaccine	Mouse 1gG2a	GP1/GP2
2G4	EBOV	2	2011	VSV/EBOV GP mouse vaccine	Mouse IgG2b	GP1/GP2
133/3.16	EBOV	3	2003	VSV/EBOV GP mouse vaccine	Mouse IgG1	GP1/GP2
16F6	SUDV	4	2011	VEE/SUDV GP mouse vaccine/irradiated virus	Mouse IgG1	GP1/GP2
1H3	EBOV	2	2011	VSV/EBOV GP mouse vaccine	Mouse 1gG2a	Glycan Cap/sGP
13C6	EBOV	5	2000	VEE/EBOV GP mouse vaccine	Mouse IgG2a	Glycan Cap/sGP
S9	EBOV	6	2014	VEE/EBOV GP	Mouse IgG unknown	Glycan Cap
13F6	EBOV	5	2000	VEE/EBOV GP mouse vaccine	Mouse IgG2a	Mucin-like domains
6D8	EBOV	5	2000	VEE/EBOV GP mouse vaccine	Mouse IgG2a	Mucin-like domains

Antibodies that are known to be protective in rodent and/or NHP models are listed, emphasizing the common themes of binding despite the mAbs' points of origin.

1. Lee JE, et al. (2008) Structure of the Ebola virus glycoprotein bound to an antibody from a human survivor. *Nature* 454(7201):177–182.
2. Qiu X, et al. (2011) Characterization of Zaire ebolavirus glycoprotein-specific monoclonal antibodies. *Clin Immunol* 141(2):218–227.
3. Takada A, et al. (2003) Identification of protective epitopes on ebola virus glycoprotein at the single amino acid level by using recombinant vesicular stomatitis viruses. *J Virol* 77(2): 1069–1074.
4. Dias JM, et al. (2011) A shared structural solution for neutralizing ebolaviruses. *Nat Struct Mol Biol* 18(12):1424–1427.
5. Wilson JA, et al. (2000) Epitopes involved in antibody-mediated protection from Ebola virus. *Science* 287(5458):1664–1666.
6. Marceau, et al. (2014) Novel neutralizing monoclonal antibodies protect rodents against lethal filovirus challenges. *Trials Vaccinol* 3:89–94.